

Mechanism and timing of Mcm2–7 ring closure during DNA replication origin licensing

Simina Ticau^{1,4}, Larry J Friedman², Kanokwan Champasa¹, Ivan R Corrêa Jr³, Jeff Gelles² & Stephen P Bell¹

The opening and closing of two ring-shaped Mcm2–7 DNA helicases is necessary to license eukaryotic origins of replication, although the mechanisms controlling these events are unclear. The origin-recognition complex (ORC), Cdc6 and Cdt1 facilitate this process by establishing a topological link between each Mcm2–7 hexamer and origin DNA. Using colocalization single-molecule spectroscopy and single-molecule Förster resonance energy transfer (FRET), we monitored ring opening and closing of *Saccharomyces cerevisiae* Mcm2–7 during origin licensing. The two Mcm2–7 rings were open during initial DNA association and closed sequentially, concomitant with the release of their associated Cdt1. We observed that ATP hydrolysis by Mcm2–7 was coupled to ring closure and Cdt1 release, and failure to load the first Mcm2–7 prevented recruitment of the second Mcm2–7. Our findings identify key mechanisms controlling the Mcm2–7 DNA-entry gate during origin licensing, and reveal that the two Mcm2–7 complexes are loaded via a coordinated series of events with implications for bidirectional replication initiation and quality control.

During eukaryotic DNA replication, origins of replication are licensed when two copies of the ring-shaped, heterohexameric Mcm2–7 helicase topologically encircle origin DNA¹. This linkage is established when the Mcm2–Mcm5 gate (the interface between Mcm2 and Mcm5) is opened to allow DNA to enter the central channel of the helicase and then closed to prevent DNA release^{2,3}. The two Mcm2–7 complexes are loaded sequentially. One Mcm2–7, in complex with Cdt1, is initially recruited to origin DNA bound by the ORC and Cdc6 (refs. 4–7). This intermediate rapidly releases Cdc6 and then Cdt1 (refs. 6,8). A second Cdc6 and the Cdt1–Mcm2–7 complex then associate with the ORC and the first Mcm2–7 (refs. 8,9), and subsequently Cdc6, Cdt1 and ORC are released⁸. The net result is a head-to-head Mcm2–7 double hexamer that encircles the origin DNA and is poised for bidirectional initiation^{4,10}.

ATP binding and hydrolysis are critical for helicase loading. ATP binding is required for the initial DNA association of the three helicase-loading proteins and Mcm2–7 (refs. 11,12). ATP hydrolysis is required for the process to move beyond this initial association and for Mcm2–7 loading to be completed^{6,13,14}. ORC, Cdc6 and Mcm2–7 all bind and hydrolyze ATP. Although not required for helicase loading, ORC ATP hydrolysis is required for the repetition of this event¹⁵. Cdc6 ATP hydrolysis also is not required for helicase loading^{13,14,16}; however, it is required for a quality control mechanism that releases incompletely loaded Mcm2–7 from DNA^{13,14,17}. Mcm2–7 ATP hydrolysis by at least a subset of the six Mcm2–7 ATPase motifs is required for helicase loading^{13,14}, but it remains unclear which event(s) depends on the action of these ATPases.

Although previous studies revealed both the order of protein associations during helicase loading and their regulation¹⁸, the timing and

mechanism of the key event of Mcm2–7 ring opening and closing have remained unclear. ATP binding at the Mcm2–Mcm5 interface is proposed to close the Mcm2–7 ring³, and this idea is supported by findings from electron microscopy studies of ATP γ S-bound Mcm2–7 (ref. 9). In contrast, structural studies have shown that Mcm2–7 is in an open state in the presence of ATP^{19,20}. The status of the Mcm2–Mcm5 gate in the initially recruited Cdt1–Mcm2–7 complex is unknown. The sequence similarity and structural similarity of ORC–Cdc6 to sliding clamp loaders have led to a hypothesis that binding to ORC and Cdc6 opens the Mcm2–7 ring⁷, but this remains to be tested.

Using a single-molecule FRET-based approach, we examined the timing and mechanism of Mcm2–7 ring opening and closing, and their relationship to other events of origin licensing. We found that Mcm2–7 is in an open state upon initial binding, and that this state is independent of Cdt1 binding. Mcm2–7 ring closure occurs independently for each Mcm2–7 at a time that is concomitant with Cdt1 release. In addition, we found that ATP hydrolysis by Mcm5–Mcm3 is required for ring closure and Cdt1 release. When these events were prevented, recruitment of the second Mcm2–7 ring was inhibited. Our findings provide important insights into the mechanism of helicase loading and reveal attributes of this event that favor double-hexameric formation and quality control.

RESULTS

An assay for Mcm2–Mcm5 gate status

Using the closed Mcm2–7 ring structure as a reference²¹, we attached donor and acceptor fluorophores to Mcm2 and Mcm5 at positions where FRET should increase in the closed state (**Fig. 1a** and **Supplementary Fig. 1a**). This fluorescent variant (Mcm2–7^{25FRET})

¹Howard Hughes Medical Institute, Department of Biology, Massachusetts Institute of Technology, Cambridge, Massachusetts, USA. ²Department of Biochemistry, Brandeis University, Waltham, Massachusetts, USA. ³New England Biolabs, Ipswich, Massachusetts, USA. ⁴Present address: VL34 Inc., Cambridge, Massachusetts, USA. Correspondence should be addressed to S.P.B. (spbell@mit.edu) or J.G. (gelles@brandeis.edu).

Received 8 September 2016; accepted 9 January 2017; published online 13 February 2017; doi:10.1038/nsmb.3375

functioned at near-wild-type levels in bulk helicase-loading assays with purified proteins (Supplementary Fig. 1b–d). To measure Mcm2–7 DNA association and changes in apparent FRET efficiency (E_{FRET}) during helicase loading, we incubated surface-attached fluorescent origin DNA with purified Mcm2–7^{25FRET}, ORC, Cdc6 and Cdt1 (ref. 8). Colocalization of the protein- and DNA-associated fluorophores was indicative of DNA binding. By using alternating excitation of the acceptor and donor fluorophores (Fig. 1b and Supplementary Figs. 2 and 3a), we were able to monitor Mcm2–7 binding to individual DNAs and calculate E_{FRET} for bound Mcm2–7^{25FRET}. Long-lived sequential increases in Mcm2–7-associated fluorescence revealed the first and second Mcm2–7 binding events⁸ (Fig. 1b and Supplementary Fig. 3a). We focused on events in which simultaneous increases in both acceptor-excited and total donor-excited fluorescence (Fig. 1b) indicated that an Mcm2–7^{25FRET} with both donor and acceptor fluorophores was binding. After initial binding, Mcm2–7^{25FRET} showed relatively high donor emission and weak acceptor emission (Fig. 1b; ~850 s), resulting in a low E_{FRET} value. Long-lived Mcm2–7^{25FRET} molecules subsequently displayed decreased donor emission and increased acceptor emission, indicative of increased E_{FRET} (Fig. 1b; ~880 s).

Analysis of a large number of Mcm2–7^{25FRET} helicase-loading trajectories revealed evidence for two major types of DNA–Mcm2–7 complexes with distinct E_{FRET} values (Fig. 1c). Early after DNA binding (<15 s), Mcm2–7^{25FRET} was predominantly in a state where $E_{\text{FRET}} \sim 0.18$ (Fig. 1c, Supplementary Fig. 3b and Supplementary Table 1). At intermediate times (15–75 s), we observed a mixture of states with $E_{\text{FRET}} \sim 0.18$ and $E_{\text{FRET}} \sim 0.36$. At longer times (>75 s), E_{FRET} values were almost all ~ 0.36 . We observed a similar set of distributions for binding of a second Mcm2–7^{25FRET}, except that an intermediate E_{FRET} value of ~ 0.28 was seen at early time points (Supplementary Fig. 3c and Supplementary Table 2). This intermediate value suggests that the first Mcm2–7 remains in the state where $E_{\text{FRET}} \sim 0.36$, whereas the second Mcm2–7 is initially in the state where $E_{\text{FRET}} \sim 0.18$. These distributions are consistent with a transition of both the first and the second Mcm2–7 complexes from an open Mcm2–Mcm5 gate ($E_{\text{FRET}} \sim 0.18$) to a closed Mcm2–Mcm5 gate ($E_{\text{FRET}} \sim 0.36$). We observed a similar transition between discrete low and high E_{FRET} states during helicase loading for an alternative Mcm2–7 construct in which Mcm2 was fluorescently labeled at a different location (Supplementary Fig. 3d). This finding is in agreement with the idea that the increase in E_{FRET} is caused by a conformational change that decreases the distance between Mcm2 and Mcm5.

Mcm2–7^{25FRET}–DNA complexes with time-averaged E_{FRET} values greater than 0.25 correlated with long-lived (>100 s) DNA associations (Fig. 1d), which supports the idea that the higher E_{FRET} state represents a closed Mcm2–Mcm5 gate. Consistent with higher E_{FRET} values being caused by changes in an individual Mcm2–7 hexamer, we observed elevated E_{FRET} values only when the donor and the acceptor were on the same Mcm2–7 (Supplementary Fig. 2a). Furthermore, once molecules reached $E_{\text{FRET}} \sim 0.36$, no persistent excursions at or below E_{FRET} values of 0.18 were observed (>5 s; $N = 0/57$), consistent with a stably closed Mcm2–7 ring⁴. These findings, combined with subsequent observations, led us to conclude that E_{FRET} values of ~ 0.18 and ~ 0.36 for individual Mcm2–7^{25FRET} complexes indicate the presence of the open and closed conformations of the Mcm2–Mcm5 gate, respectively.

Cdt1 release is concomitant with Mcm2–7 ring closure

Because Cdc6 and Cdt1 sequentially dissociate from DNA after facilitating the initial Mcm2–7 binding⁸, we asked whether either

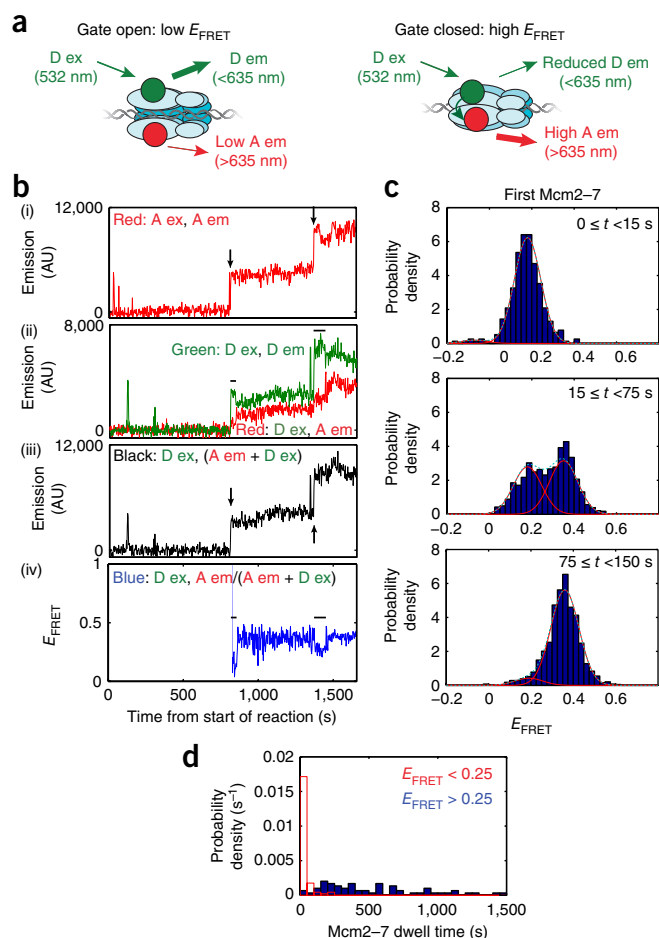


Figure 1 Mcm2–7 hexamers associate with DNA while in an open-gate conformation and subsequently close. (a) Schematic of DNA-bound Mcm2–7^{25FRET} in the open-gate and closed-gate states. Mcm2 and Mcm5 were labeled with acceptor (A; red circles) and donor (D; green circles) fluorophores, respectively. Mcm2–Mcm5 gate closure increased the proximity of the fluorophores and the FRET efficiency (E_{FRET}). Fluorescence excitation (ex) and emission (em) wavelengths are indicated. (b) Example traces for Mcm2–7^{25FRET} association with origin DNA. Acceptor-excited (i) and donor-excited (ii) emission records are shown together with calculated donor-excited total emission (iii) and E_{FRET} (iv). Black arrows show the initial association of long-lived Mcm2–7^{25FRET}. Black horizontal bars indicate low- E_{FRET} intervals observed at the beginning of these associations. AU, arbitrary units. (c) Histograms of E_{FRET} values recorded during the indicated time intervals after association of the first Mcm2–7^{25FRET} with origin DNA. Fits to the sum (dashed cyan curves) of two Gaussians (red curves) yielded the fit parameters reported in Supplementary Table 1. For accurate E_{FRET} determination, we analyzed only the 51 first Mcm2–7 associations that retained donor and acceptor fluorophores for >150 s and that lacked a second Mcm2–7 association within 150 s of DNA association. The same molecules were used for each histogram, and data from 255 (0–15 s), 1,020 (15–75 s) and 1,320 (75–150 s) total time points were plotted. (d) Histogram of single Mcm2–7 dwell times. Mcm2–7 associations with a time-averaged $E_{\text{FRET}} < 0.25$ ($N = 91$ molecules) are plotted in red, and those with a time-averaged $E_{\text{FRET}} > 0.25$ ($N = 59$ molecules) are in blue. Time-averaged E_{FRET} was calculated over the duration of the association or until the association of a second Mcm2–7. For 29 molecules with average $E_{\text{FRET}} > 0.25$, the measured dwell times were truncated by the end of the recording.

of these events is correlated with Mcm2–Mcm5 gate closure. For the first Mcm2–7 association, we compared the time of gate closure, defined as the point at which E_{FRET} reached ~ 0.36 , with previously

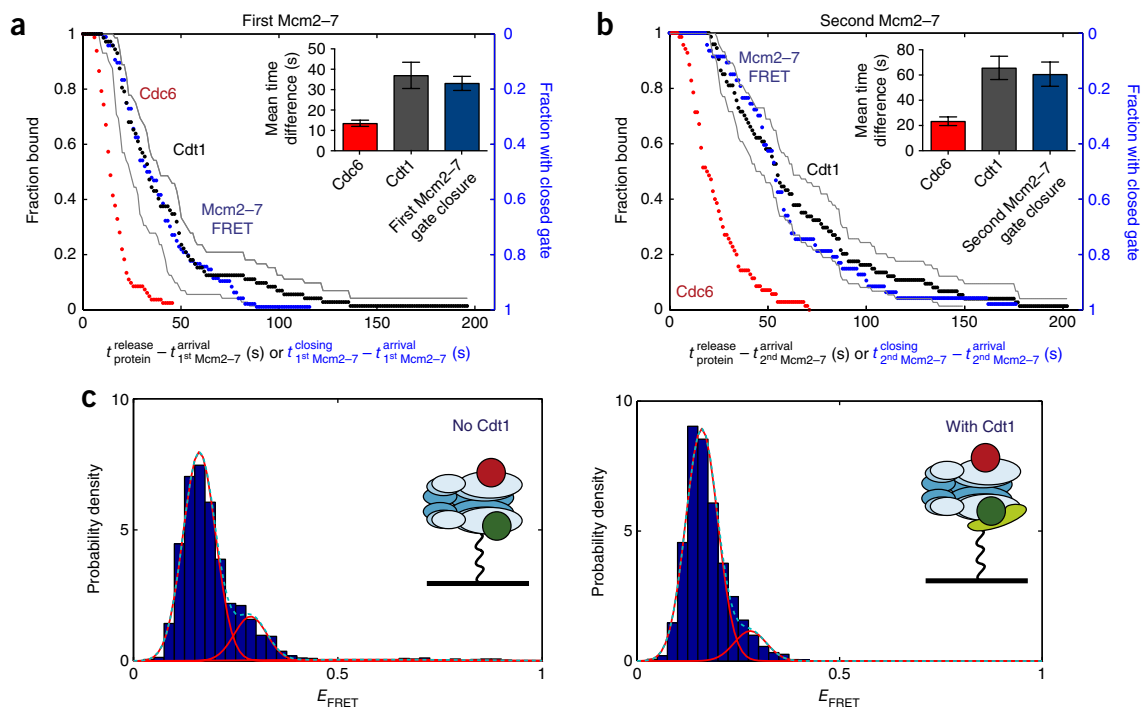


Figure 2 Mcm2-7 gate closure correlates with the release of Cdt1 on DNA but not free in solution. **(a)** The fraction of dye-labeled Cdc6 ($N = 96$ molecules) or Cdt1 ($N = 72$ molecules) bound at various times after the first Mcm2-7 association (from ref. 8) (marked along the left-hand vertical axis) and the fraction of Mcm2-7^{25FRET} molecules showing gate closure (Mcm2-7 FRET; $N = 96$ molecules) at various times (marked along the right-hand vertical axis). The 95% confidence interval (CI) for the time of Cdt1 release is indicated by the gray solid lines. The inset shows the mean release times and gate-closure time ($\pm 95\%$ CI). Gate-closure times were based on the first time point at which the E_{FRET} value increased by 0.15 over the average of five previous time points and was sustained for at least five time points. **(b)** The same as in **a**, but for events after association with the second Mcm2-7^{25FRET}. The closed-gate fraction ($N = 47$ molecules) is shown on the right-hand vertical axis. The release of Cdc6 ($N = 70$ molecules) and Cdt1 ($N = 74$ molecules; 95% CI indicated by gray solid lines) can be assessed with the left-hand vertical axis (from ref. 8). Gate-closure times were determined as in **a**, except that the E_{FRET} increase threshold was 0.1. **(c)** Histograms of E_{FRET} values of tethered Mcm2-7^{25FRET} in either the absence ($N = 32$ molecules, 2,014 total time points) or the presence ($N = 60$ molecules, 3,712 total time points) of Cdt1, fit with the sum (cyan dashed line) of two (with Cdt1) or three (no Cdt1) Gaussians (red curves), which yielded the fit parameters reported in **Supplementary Table 3**. The presence of Cdt1 moderately increased the percentage of Mcm2-7 in the open ($E_{\text{FRET}} \sim 0.16$) state (88% versus 80%). In both cases, the majority of the remaining data fit to a second state with $E_{\text{FRET}} \sim 0.28$, which is likely to represent a partially closed Mcm2-Mcm5 gate. Insets show schemes of attachment. Mcm2-7^{25FRET} was tethered to the slide surface either directly through the Mcm5 subunit (no Cdt1; Mcm2-7^{25FRET}-biotin) or indirectly through biotinylated Cdt1 tethered to the surface (with Cdt1).

determined distributions of first Cdc6 and Cdt1-release times (Fig. 2a and ref. 8). In each case, we measured these times relative to the initial Mcm2-7-DNA association. The average time to Cdc6 release was much shorter than the average gate-closure time. In contrast, the distributions of times to Cdt1 release and to gate closure were similar, thus supporting a connection between these events. Because Cdt1 is released more slowly for the second Mcm2-7 than for the first⁸, we asked whether Mcm2-Mcm5 gate closure for the second Mcm2-7 is similarly delayed. Indeed, the gate-closure times after the arrival of the second Mcm2-7 showed a distribution similar to that for the second Cdt1 release (Fig. 2b). Thus, for both the first and the second Mcm2-7, ring closure was concomitant with Cdt1 release.

For comparisons between previously determined Cdt1-release times and Mcm2-7^{25FRET} ring-closure times to be valid, the kinetics of the Mcm2-7^{25FRET} loading reaction should be similar to that for the singly modified Mcm2-7 (Mcm2-7 with SNAP at the N terminus of Mcm4 (Mcm2-7^{4SNAP})) used in the previous determination of Cdt1-release times⁸. To test for this, we made Mcm2-7^{25FRET*}, a preparation in which Mcm5-SNAP is attached to a fluorophore but Mcm2-CLIP is still present in the complex. With only a single fluorophore on Mcm2-7^{25FRET*}, we could simultaneously measure the association and dissociation with DNA of Mcm2-7^{25FRET*} and a second protein labeled with a second fluorophore. Although helicase loading

was inhibited when Mcm2-7^{25FRET*} was combined with labeled Cdt1, labeled ORC and Cdc6 were compatible with Mcm2-7^{25FRET*}. Importantly, we observed similar release times for Cdc6 and ORC whether we used Mcm2-7^{25FRET*} or Mcm2-7^{4SNAP} (Supplementary Fig. 4a-c). Although we could not measure the kinetics of Cdt1 in the presence of Mcm2-7^{25FRET}, we note that the times of Cdc6 and ORC release encompassed the times of Cdt1 release. Thus, the kinetics of the helicase loading reaction was not dramatically changed by the SNAP and CLIP proteins in Mcm2-7^{25FRET}.

The similar kinetics of Cdt1 release and Mcm2-7 ring closure suggested that the binding of Cdt1 to Mcm2-7 holds the Mcm2-Mcm5 gate open. To address this possibility, we monitored E_{FRET} for Mcm2-7^{25FRET} in the absence of DNA, ORC and Cdc6. Whether Mcm2-7^{25FRET} was directly tethered to the slide in the absence of Cdt1 or tethered to the slide indirectly via Cdt1, the Mcm2-Mcm5 gate was predominantly in an open ($E_{\text{FRET}} \sim 0.16$) state, with smaller populations in higher E_{FRET} states (Fig. 2c and Supplementary Table 3). Interestingly, Cdt1-bound Mcm2-7 showed a smaller fraction of molecules in the higher E_{FRET} states (Supplementary Table 3), which suggests that Cdt1 increases the already high likelihood that Mcm2-7 will adopt an open ($E_{\text{FRET}} \sim 0.16$) conformation. In agreement with the hypothesis that Mcm2-7 exists mostly in an open state when in complex with Cdt1, in contrast to the closed state of

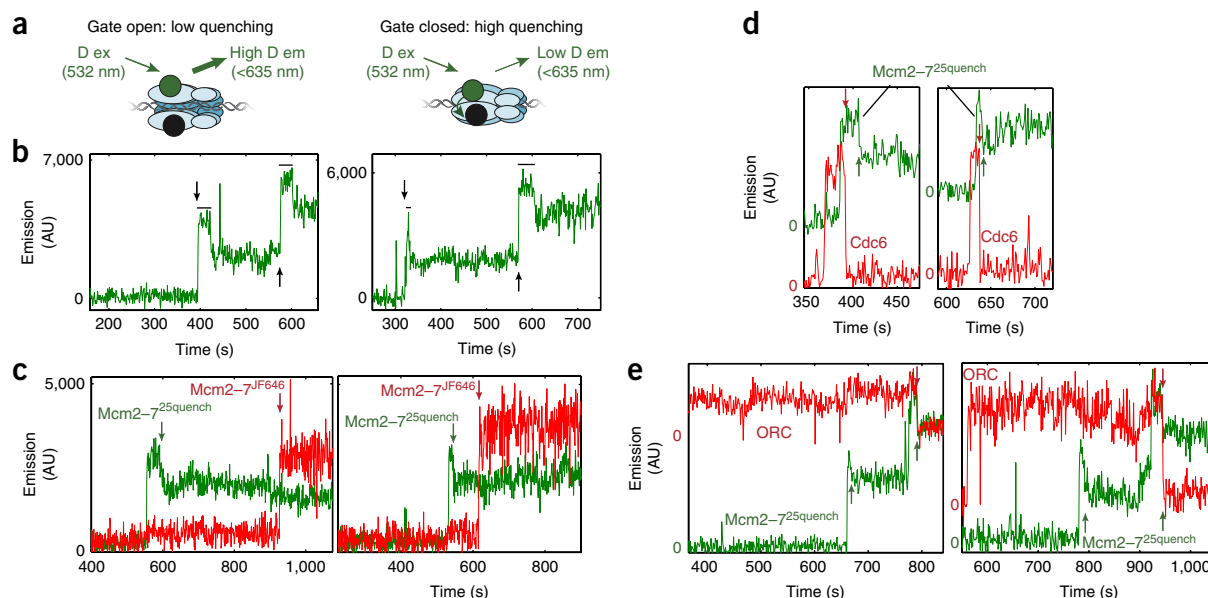


Figure 3 Closure of the second Mcm2–7 ring correlates with ORC release. **(a)** Schematic of Mcm2–7^{25quench} labeling in the open-gate and closed-gate states. Mcm2 and Mcm5 were labeled with donor fluorophore (D; green circles) and quencher (BHQ-2; black circles), respectively. Closure of the Mcm2–Mcm5 gate decreases the distance between the fluorophore and quencher, and thus decreases donor emission. **(b)** Two example traces showing sequential association of two Mcm2–7^{25quench} molecules with individual origin DNA molecules. The black arrows show the initial association of long-lived Mcm2–7^{25quench}. The black horizontal bars indicate intervals of no or low quenching after the first and second Mcm2–7^{25quench} associations. **(c)** DNA-molecule colocalization fluorescence records for experiments with a mixture of labeled Mcm2–7 (Mcm2–7^{JF646}) and Mcm2–7^{25quench}. To investigate whether there were changes in the status of the first Mcm2–Mcm5 gate during loading of the second Mcm2–7, we examined examples in which the first bound hexamer was Mcm2–7^{25quench} and the second bound hexamer was Mcm2–7^{JF646}. In both cases, Mcm2–7^{25quench} closed before the arrival of Mcm2–7^{JF646} (green arrows), and its quenching state did not change when an Mcm2–7^{JF646} was bound as the second Mcm2–7 hexamer (red arrows). **(d)** Representative DNA-molecule colocalization fluorescence records for experiments using labeled Cdc6^{SORT549} and Mcm2–7^{25quench}. In each record, Cdc6 release (red arrows) occurred before an increase in Mcm2–7 quenching (green arrows). The calculated mean dwell time of Cdc6 (12.0 ± 2.2 s (mean \pm s.e.m.)) is more than five-fold shorter than the mean photobleaching lifetime of the Cdc6-bound fluorophore under these conditions (77 ± 18 s (mean \pm s.e.m.))⁸, which indicates that most disappearances were due to Cdc6 DNA release, not photobleaching. Note: Mcm2–7^{25quench} records are vertically offset to facilitate comparison. **(e)** Representative DNA-molecule colocalization fluorescence records for experiments using labeled ORC^{1SORT549} and Mcm2–7^{25quench}. In each record, ORC release (red arrows) occurred simultaneously with the second Mcm2–7 quenching increase (green arrows). Note: ORC records are vertically offset to facilitate comparison. AU, arbitrary units.

loaded Mcm2–7, we measured solution E_{FRET} values for free Cdt1–Mcm2–7^{25FRET} and loaded Mcm2–7^{25FRET}. Although the absolute values were different from those seen in the single-molecule experiments owing to incomplete protein labeling (only doubly labeled proteins were assessed in the single-molecule setting), we observed higher solution E_{FRET} values for loaded Mcm2–7^{25FRET} (0.129 ± 0.004) than for free Cdt1–Mcm2–7^{25FRET} (0.076 ± 0.002). These findings agree with the results of previous low-resolution structural studies showing that free Mcm2–7 has an open Mcm2–Mcm5 gate^{19,20}. We conclude that Cdt1 is not required to prevent Mcm2–7 ring closure, but Cdt1-bound Mcm2–7 may more strongly favor the open state.

ORC release occurs after closure of both Mcm2–7 rings

To simultaneously monitor the status of the Mcm2–Mcm5 gate and release of fluorescently labeled proteins from individual DNAs in three-color experiments, we labeled Mcm2 and Mcm5 with a fluorophore and a quencher, respectively (Mcm2–7^{25quench}; **Fig. 3a**). Bulk assays showed that Mcm2–7^{25quench} retained ~50% of wild-type helicase-loading activity (**Supplementary Fig. 1c,d**). Consistent with our Mcm2–7^{25FRET} studies, this complex showed high fluorescence upon initial DNA binding (open gate) and reduced fluorescence thereafter (closed gate; **Fig. 3b** and **Supplementary Fig. 4d**). Experiments in which we combined Mcm2–7^{25quench} with differentially labeled Mcm2–7 (Mcm2–7^{JF646}) showed that the Mcm2–Mcm5 gate of the

first Mcm2–7 did not reopen once closed, including during loading of the second Mcm2–7 (**Fig. 3c**).

As with Mcm2–7^{25FRET}, labeled Cdc6 and ORC were compatible with Mcm2–7^{25quench}, but fluorescently labeled Cdt1 inhibited helicase loading when combined with this form of Mcm2–7. In agreement with previous results⁸ showing that Cdc6 is released before Cdt1, labeled Cdc6 was always released before Mcm2–7^{25quench} gate closure (**Fig. 3d**; 62/62 events). When we combined labeled ORC with Mcm2–7^{25quench}, we noted a connection between ORC release and closing of the second Mcm2–7 ring. In the majority of events (47/54), the single ORC involved in helicase loading⁸ was released at a time within the range of experimental error for gate closure of the second Mcm2–7 (**Fig. 3e**). In the remaining events, ORC was retained on the DNA after the second ring closure. Interestingly, the average time until the second Mcm2–7 ring closure was much longer than the previously determined average time until the establishment of Mcm2–7–Mcm2–7 double-hexamer interactions (as measured by FRET between the N termini of the first and second Mcm2–7 hexamers⁸; **Supplementary Fig. 4e**). Thus, an open second Mcm2–7 ring engages in initial double-hexamer interactions with a closed first Mcm2–7 ring (**Fig. 3c**), which raises the possibility that the closed first Mcm2–7 ring could act as a template to facilitate closing of the second Mcm2–7 ring. Taken together, our data strongly suggest that ORC release occurs only after the formation of the Mcm2–7 double hexamer and closure of both

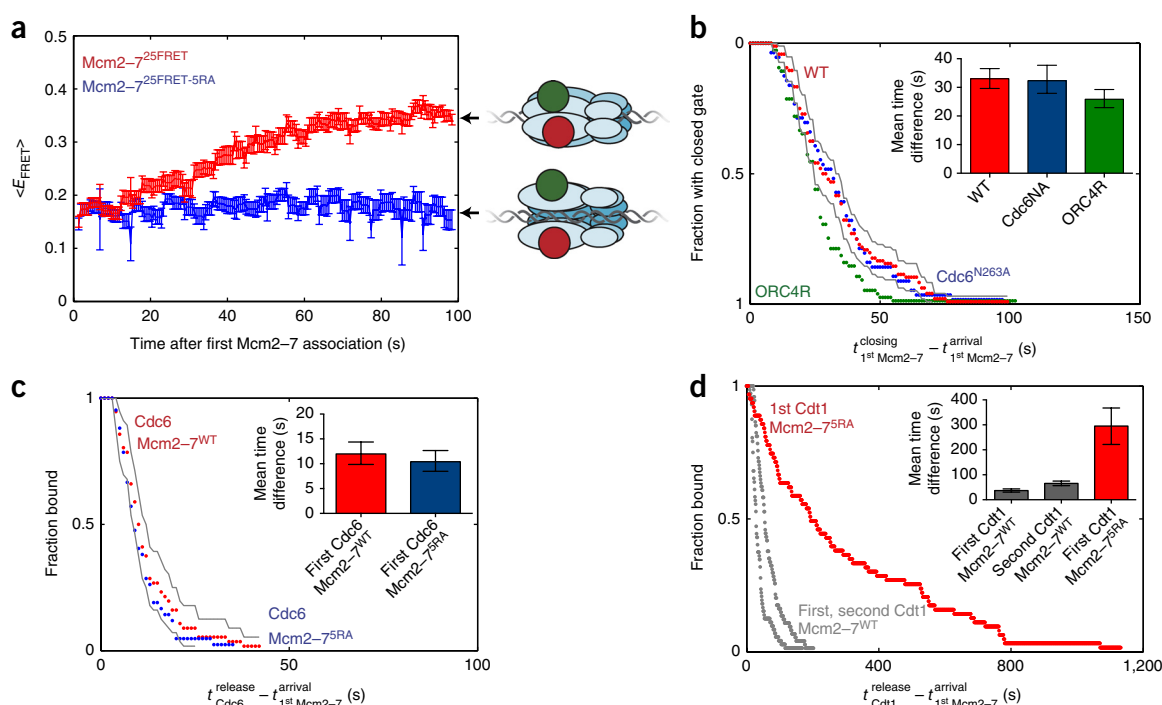


Figure 4 Mcm2-7 ATP hydrolysis is required for gate closure and Cdt1 release. (a) Comparison of population-average E_{FRET} values at indicated times after DNA association with the first Mcm2-7^{25FRET} ($N = 57$ molecules; same data as in **Supplementary Fig. 2b**) or Mcm2-7^{25FRET-5RA} ($N = 33$ molecules). (b) Time to gate closure after the first Mcm2-7^{25FRET}-DNA association for reactions with wild-type (WT) ORC-Cdc6 ($N = 96$ molecules; 95% CI indicated by gray solid lines), ORC-Cdc6^{N263A} ($N = 56$ molecules) or ORC4R-Cdc6 ($N = 75$ molecules). The inset shows the mean gate closure times ($\pm 95\%$ CI). (c) Time to Cdc6^{SORT549} release after association of the first Mcm2-7^{WT} (data from ref. 8; $N = 56$ molecules; 95% CI indicated by gray solid lines) or Mcm2-7^{5RA} ($N = 42$ molecules) hexamers. The inset shows the mean release times ($\pm 95\%$ CI). (d) Times (data from ref. 8) of Cdt1^{SORT549} release after the arrival of the first ($N = 72$) and second ($N = 74$ molecules) Mcm2-7^{WT} compared to times of Cdt1^{SORT549} release after arrival of the first Mcm2-7^{5RA} ($N = 63$ molecules). The inset shows the mean release times ($\pm 95\%$ CI). The release times for Mcm2-7^{5RA}-associated Cdt1 were underestimated because of associations that remained when the imaging ended (32 of 63 molecules) and because of Cdt1^{SORT549} photobleaching effects.

Mcm2-7 rings; such a mechanism would ensure that ORC is retained until the completion of origin licensing.

Mcm2-7 ATP hydrolysis is required for Cdt1 release and ring closure

To further investigate the mechanism of Mcm2-Mcm5 gate closure, we asked whether the ATPase activity of Mcm2-7, Cdc6 or ORC controls this event. Given the temporal connection between gate closure and Cdt1 release, we focused on a mutation in the Mcm5-Mcm3 ATPase active site (*mcm5-R549A*; **Supplementary Fig. 5a**) that leads to defects in Cdt1 release and Mcm2-7 loading^{13,14}. We incorporated this mutant into Mcm2-7^{25FRET} (Mcm2-7^{25FRET-5RA}) and monitored the status of the Mcm2-Mcm5 gate. Strikingly, Mcm2-7^{25FRET-5RA} remained in an open-gate state ($E_{\text{FRET}} \sim 0.18$) indefinitely after DNA association (**Fig. 4a** and **Supplementary Fig. 5b**). In contrast, Mcm2-Mcm5 gate closure was not prevented in Cdc6 (Cdc6^{N263A}; ref. 22) or ORC¹⁵ ATPase mutants (ORC4R; **Fig. 4b**). The kinetics of Cdc6 release was unchanged with Mcm2-7^{5RA} (**Fig. 4c**). In contrast, the dwell time for Cdt1 associated with Mcm2-7^{5RA} was dramatically extended relative to that for wild-type Mcm2-7 (**Fig. 4d**). In most cases (87/109), Cdt1-DNA association lasted as long as Cdt1-Mcm2-7^{5RA} association; this included many long-lived associations that ended with the simultaneous release of Mcm2-7 and Cdt1 (**Supplementary Fig. 5c**), as would be expected if the lack of Cdt1 release prevented ring closure. Interestingly, we did not observe any second Mcm2-7 associations (0/109) for the Mcm2-7^{5RA} mutant,

which suggests that the release of Cdt1 and/or ring closure must be complete before the second Mcm2-7 can be recruited.

DISCUSSION

Our results support our initial conclusion that Mcm2-7^{25FRET} E_{FRET} values of ~ 0.18 and ~ 0.36 represent the open and closed states of the Mcm2-Mcm5 gate, respectively. The Mcm2-7 ring was at $E_{\text{FRET}} \sim 0.18$ before and immediately after DNA binding, in agreement with the idea of an open Mcm2-7 ring allowing DNA access to the central channel. Similarly, all DNA-associated Mcm2-7^{25FRET-5RA} molecules were in the open ($E_{\text{FRET}} \sim 0.18$) state and were released by a high-salt wash that removed incompletely loaded Mcm2-7 (32/32 events)^{12,23}. In agreement with this conclusion, recent high-resolution cryo-EM structural studies of Mcm2-7 and Cdt1-Mcm2-7 showed that both complexes are in an open-ring conformation²⁴. The Mcm2-7 ATPase, but not the ORC or Cdc6 ATPases, is required for helicase loading^{13,14}. Consistent with the theory that the higher E_{FRET} state reflects a loaded, closed-ring Mcm2-7, the Mcm5-Mcm3 ATPase mutant—but not mutations in ORC or Cdc6 ATPases—prevented the formation of this state. Future studies will be required to determine whether other Mcm2-7 ATPase mutants have the same effect. Finally, attainment of $E_{\text{FRET}} \sim 0.36$ occurred independently for each Mcm2-7 complex, in agreement with evidence that the hexamers are loaded one at a time⁶⁻⁹. Although structural studies of the loaded double hexamer suggest a completely closed Mcm2-7 ring²¹, our findings do not exclude the possibility that the closed state we observed in

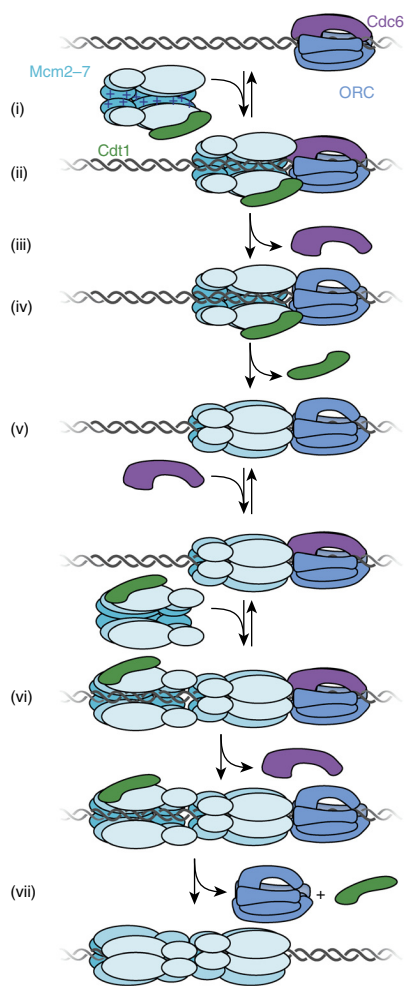


Figure 5 A model showing how the opening and closing of the Mcm2–7 gate might be controlled. Before DNA binding, the Mcm2–7 ring exists predominantly in an open conformation, probably mediated by its positively charged central channel and bound Cdt1 (i). The association of Mcm2–7 with DNA eliminates charge repulsion, and Cdt1 (perhaps with ORC–Cdc6) prevents ring closure (ii). The subsequent release of Cdc6 occurs before gate closure (iii). Closure of the first Mcm2–7 ring requires ATP hydrolysis by the Mcm5–Mcm3 ATPase (and perhaps other Mcm2–7 ATPases) (iv), and this closure event is associated with the release of Cdt1 (v). After the recruitment of a second Cdc6, a second open Cdt1–Mcm2–7 ring is recruited via interactions with the first Mcm2–7 (ref. 8) in a closed state (vi). The subsequent release of the second Cdc6 is followed by the closure of the second Mcm2–7 ring, which occurs simultaneously with the release of Cdt1 and ORC (vii).

FRET experiments is sufficiently open to allow single-stranded DNA to escape the loaded double hexamer.

In addition to revealing the times of Mcm2–7 ring closure during helicase loading, the concomitant release of Cdt1 and closure of the Mcm2–Mcm5 gate, and the inhibition of both events by the Mcm5–Mcm3 ATPase mutant, support a model in which these events are causally linked (Fig. 5). We propose that the positively charged Mcm2–7 central channel and Cdt1 binding (Fig. 2c and Supplementary Table 3) favor an open conformation of the Mcm2–7 ring off the DNA. ORC–Cdc6 recruits an open Cdt1–Mcm2–7 ring such that it encircles DNA⁷, similar to what was observed in recent studies of archaeal MCM loading²⁵. Although Cdt1 binding was not required for Mcm2–7 to remain in the open state off DNA, we propose

that Cdt1 holds the Mcm2–7 ring open after negatively charged DNA binds to the positively charged Mcm2–7 central channel. Finally, we propose that after Cdc6 is released, Mcm5–Mcm3 ATP hydrolysis (and perhaps other Mcm2–7 ATPases) stimulates Cdt1 release, thus triggering Mcm2–Mcm5 gate closure. It is also possible that Mcm5–Mcm3 ATP hydrolysis directly stimulates ring closure, which causes Cdt1 release. Although ORC–Cdc6 has been proposed to function like a sliding-clamp loader during helicase loading⁷, the only known sliding-clamp function²⁶ this complex seems to retain is the function of recruiting a protein ring to DNA. ORC and Cdc6 are not required for Mcm2–7 ring opening (Figs. 1 and 3), and ATP hydrolysis by ORC or Cdc6 is not required for ring closure (Fig. 4b). This does not eliminate other possible roles for ORC–Cdc6, including stimulation of Mcm2–7 ATP hydrolysis⁶ or alteration of the Mcm2–7 conformation to facilitate ring closure⁷.

The ordered release of Cdc6 and Cdt1 and the connection of the latter event to ring closure create a window of time for Mcm2–7 loading quality control^{13,14,17}. Cdc6 ATP hydrolysis is connected to the release of nonproductive Mcm2–7 complexes^{13,14}. Because the Mcm2–7 ring is open throughout Cdc6–DNA association (Fig. 3d), this quality control mechanism would not require reopening of the Mcm2–7 ring. In addition, the ordered closure of rings would allow the first and second Mcm2–7 complexes to be assessed separately. Although the mechanism of this release is unclear, one simple hypothesis is that an ATP-dependent release of Cdc6 before Mcm2–7 ring closure leads to the simultaneous release of open, nonproductive Mcm2–7 complexes.

Our findings indicate that loading of the two Mcm2–7 complexes associated with origin licensing is the result of a single coordinated event rather than two independent Mcm2–7 loading events. Both the lack of a second Mcm2–7 association for the Mcm2–7^{5RA} mutant and the finding that gate closure in the first Mcm2–7 always preceded DNA association with the second Mcm2–7 (Fig. 1b and Supplementary Fig. 2a; 47/47 events) strongly suggest that recruitment of the second Mcm2–7 cannot begin until the first loading event is completed. This is inconsistent with models that suggest that two ORC molecules independently recruit and load one Mcm2–7. The connection between ORC release and closure of the second but not the first Mcm2–7 ring (Fig. 3e) also supports the idea of a coordinated mechanism. Importantly, these properties would ensure that single Mcm2–7 loading events occurred only as the first step in the formation of an Mcm2–7 double hexamer.

The combination of fully reconstituted biochemical assays²⁷ and detailed structural models of key replication intermediates^{7,9,21} has provided important insights into the events of eukaryotic replication initiation. Single-molecule studies complement these approaches by revealing reaction kinetics that are difficult to assay in asynchronous bulk reactions, by identifying intermediates that are too short-lived or dynamic to be analyzed structurally, and by monitoring changes in protein conformation in real time. Our findings show how the combination of single-molecule colocalization and single-molecule FRET can be used to elucidate the complex and coordinated protein dynamics of helicase-loading events. More important, our findings reveal features of origin licensing that can reduce the number of incomplete or incorrect events, and thus improve genome stability.

METHODS

Methods, including statements of data availability and any associated accession codes and references, are available in the [online version of the paper](#).

Note: Any Supplementary Information and Source Data files are available in the [online version of the paper](#).

ACKNOWLEDGMENTS

We are grateful to the members of the Bell laboratory for useful discussions, B. Sauer for comments on the manuscript, and L.D. Lavis (Janelia Research Campus, Ashburn, Virginia, USA) for providing Janelia fluorophores. This work was supported by the NIH (grants R01 GM52339 (to S.P.B.) and R01 GM81648 (to J.G.); pre-doctoral training grant GM007287 to S.T.) and the G. Harold and Leila Y. Matthews Foundation (grant to J.G.). S.P.B. is an investigator with the Howard Hughes Medical Institute. This work was supported in part by the Koch Institute (support grant P30-CA14051 from the NCI to T. Jacks, Koch Institute for Integrative Cancer Research, MIT, Cambridge, Massachusetts, USA). We thank the Koch Institute Swanson Biotechnology Center for technical support, specifically the Biopolymers and Genomics cores.

AUTHOR CONTRIBUTIONS

S.T. performed all experiments with feedback from J.G., L.J.F. and S.P.B., except for the ensemble FRET studies, which were performed by K.C. I.R.C. prepared essential reagents. S.T., L.J.F. and J.G. analyzed the data. S.P.B. wrote the paper with input from all other authors. S.P.B. and J.G. directed the project.

COMPETING FINANCIAL INTERESTS

The authors declare no competing financial interests.

Reprints and permissions information is available online at <http://www.nature.com/reprints/index.html>.

- Yardimci, H. & Walter, J.C. Prereplication-complex formation: a molecular double take? *Nat. Struct. Mol. Biol.* **21**, 20–25 (2014).
- Samel, S.A. *et al.* A unique DNA entry gate serves for regulated loading of the eukaryotic replicative helicase MCM2-7 onto DNA. *Genes Dev.* **28**, 1653–1666 (2014).
- Bochman, M.L. & Schwacha, A. The Mcm2-7 complex has in vitro helicase activity. *Mol. Cell* **31**, 287–293 (2008).
- Remus, D. *et al.* Concerted loading of Mcm2-7 double hexamers around DNA during DNA replication origin licensing. *Cell* **139**, 719–730 (2009).
- Aparicio, O.M., Weinstein, D.M. & Bell, S.P. Components and dynamics of DNA replication complexes in *S. cerevisiae*: redistribution of MCM proteins and Cdc45p during S phase. *Cell* **91**, 59–69 (1997).
- Fernández-Cid, A. *et al.* An ORC/Cdc6/MCM2-7 complex is formed in a multistep reaction to serve as a platform for MCM double-hexamer assembly. *Mol. Cell* **50**, 577–588 (2013).
- Sun, J. *et al.* Cryo-EM structure of a helicase loading intermediate containing ORC–Cdc6–Cdt1–MCM2-7 bound to DNA. *Nat. Struct. Mol. Biol.* **20**, 944–951 (2013).
- Ticau, S., Friedman, L.J., Ivica, N.A., Gelles, J. & Bell, S.P. Single-molecule studies of origin licensing reveal mechanisms ensuring bidirectional helicase loading. *Cell* **161**, 513–525 (2015).
- Sun, J. *et al.* Structural and mechanistic insights into Mcm2-7 double-hexamer assembly and function. *Genes Dev.* **28**, 2291–2303 (2014).
- Evrin, C. *et al.* A double-hexameric MCM2-7 complex is loaded onto origin DNA during licensing of eukaryotic DNA replication. *Proc. Natl. Acad. Sci. USA* **106**, 20240–20245 (2009).
- Bell, S.P. & Stillman, B. ATP-dependent recognition of eukaryotic origins of DNA replication by a multiprotein complex. *Nature* **357**, 128–134 (1992).
- Randell, J.C.W., Bowers, J.L., Rodríguez, H.K. & Bell, S.P. Sequential ATP hydrolysis by Cdc6 and ORC directs loading of the Mcm2-7 helicase. *Mol. Cell* **21**, 29–39 (2006).
- Kang, S., Warner, M.D. & Bell, S.P. Multiple functions for Mcm2-7 ATPase motifs during replication initiation. *Mol. Cell* **55**, 655–665 (2014).
- Coster, G., Frigola, J., Beuron, F., Morris, E.P. & Diffley, J.F.X. Origin licensing requires ATP binding and hydrolysis by the MCM replicative helicase. *Mol. Cell* **55**, 666–677 (2014).
- Bowers, J.L., Randell, J.C.W., Chen, S. & Bell, S.P. ATP hydrolysis by ORC catalyzes reiterative Mcm2-7 assembly at a defined origin of replication. *Mol. Cell* **16**, 967–978 (2004).
- Chang, F. *et al.* Cdc6 ATPase activity disengages Cdc6 from the pre-replicative complex to promote DNA replication. *eLife* **4**, 1–42 (2015).
- Frigola, J., Remus, D., Mehanna, A. & Diffley, J.F.X. ATPase-dependent quality control of DNA replication origin licensing. *Nature* **495**, 339–343 (2013).
- Deegan, T.D. & Diffley, J.F. MCM: one ring to rule them all. *Curr. Opin. Struct. Biol.* **37**, 145–151 (2016).
- Costa, A. *et al.* The structural basis for MCM2-7 helicase activation by GINS and Cdc45. *Nat. Struct. Mol. Biol.* **18**, 471–477 (2011).
- Lyubimov, A.Y., Costa, A., Bleichert, F., Botchan, M.R. & Berger, J.M. ATP-dependent conformational dynamics underlie the functional asymmetry of the replicative helicase from a minimalist eukaryote. *Proc. Natl. Acad. Sci. USA* **109**, 11999–12004 (2012).
- Li, N. *et al.* Structure of the eukaryotic MCM complex at 3.8 Å. *Nature* **524**, 186–191 (2015).
- Schepers, A. & Diffley, J.F. Mutational analysis of conserved sequence motifs in the budding yeast Cdc6 protein. *J. Mol. Biol.* **308**, 597–608 (2001).
- Donovan, S., Harwood, J., Drury, L.S. & Diffley, J.F. Cdc6p-dependent loading of Mcm proteins onto pre-replicative chromatin in budding yeast. *Proc. Natl. Acad. Sci. USA* **94**, 5611–5616 (1997).
- Zhai, Y. *et al.* Open-ringed structure of the Cdt1–MCM2-7 complex as a precursor of the MCM double hexamer. *Nat. Struct. Mol. Biol.* <http://dx.doi.org/10.1038/nsmb.3374> (2016).
- Samson, R.Y., Abeyrathne, P.D. & Bell, S.D. Mechanism of Archaeal MCM helicase recruitment to DNA replication origins. *Mol. Cell* **61**, 287–296 (2016).
- Kelch, B.A. The lord of the rings: structure and mechanism of the sliding clamp loader. *Biopolymers* **105**, 532–546 (2016).
- Yeeles, J.T.P., Deegan, T.D., Janska, A., Early, A. & Diffley, J.F.X. Regulated eukaryotic DNA replication origin firing with purified proteins. *Nature* **519**, 431–435 (2015).

ONLINE METHODS

Protein expression and purification strains. Cdc6^{SORT549} (pET-GSS-Cdc6), Cdt1^{SORT549-Mcm2-74SNAP} (yST166) and ORC^{SORT549} (yST163) were purified as described previously⁸. To monitor the Mcm2-Mcm5 gate, we constructed strains that expressed Cdt1-Mcm2-7^{25FRET}, by introducing an Asc I site after amino acid 721 of Mcm2 and amino acid 591 of Mcm5 (ref. 2). A SNAP-tag (Mcm5, NEB) or CLIP-tag (Mcm2, NEB) was inserted with ten amino acid linkers (GGSGGGSGG) at each junction. For purification of Mcm2-7^{25FRET}, Mcm2-721^{CLIP} and Mcm5-591^{SNAP} were expressed in conjunction with the remaining wild-type Mcm2-7 subunits and Cdt1 (yST229) or in the absence of Cdt1 (yST266, to make Mcm2-7^{25FRET}-biotin) and labeled with CLIP-Surface 647 (NEB) and SNAP-Surface 549 (NEB) as described below. To monitor gate closure by quenching (Mcm2-7^{25quench}) or to create an alternate Mcm2-Mcm5 gate FRET pair (Mcm2-7^{25FRET}), we coexpressed Mcm2^{SORT} (Mcm2 with LPETGG at its C terminus) and Mcm5-591^{SNAP} with the remaining wild-type Mcm2-7 subunits and Cdt1 (yST220). We used Sortase to attach Mcm2^{SORT} to the peptide NH₂-GGGHHHHHHHHHC-COOH coupled to maleimide-Dy549, and we coupled Mcm5-591^{SNAP} to SNAP-BHQ-2 to form Mcm2-7^{25quench} (see below) or to SNAP-Surface 649 to form Mcm2-7^{25FRET}. Mcm2-Mcm5 gate FRET was monitored in the context of the Mcm5-R549A mutant protein by incorporating the mutation into Mcm5 subunit of the strain expressing Cdt1-Mcm2-7^{25FRET} (yST299). The resulting mutant Cdt1-Mcm2-7 was labeled as described for Mcm2-7^{25FRET} to form Mcm2-7^{25FRET-mcm5RA}. We monitored the effect of Mcm5-R549A on Cdt1 release by purifying Cdt1-Mcm2-7 from a strain that expressed Mcm5-R549A, Mcm4^{SNAP}, Cdt1^{SORT} and the remaining wild-type Mcm subunits (yST291). Mcm4^{SNAP} was labeled with SNAP-JF646 (a gift from Luke Lavis, Janelia Research Campus), and Cdt1^{SORT} was coupled to the peptide NH₂-GGGHHHHHHHHHC-COOH coupled to maleimide-Dy549 to make Cdt1^{SORT549-Mcm2-74SNAP-mcm5RA}. We monitored the effect of Mcm5-R549A on Cdc6 release by purifying Cdt1-Mcm2-7 from a strain that expressed Mcm5-R549A, Mcm4^{SNAP}, Cdt1 and the remaining wild-type Mcm subunits (yST289) to make Cdt1-Mcm2-7^{4SNAP-mcm5RA}.

Purification and fluorescent labeling of Cdt1-Mcm2-7. *S. cerevisiae* (W303 background) strains yST229, yST220, yST299 or yST291 were grown to OD₆₀₀ = 1.2 in 8 L of YEP supplemented with 2% glycerol (v/v) at 30 °C. Addition of 2% galactose (w/v) and α -factor (100 ng/mL) induced Cdt1-Mcm2-7 expression and arrested cells at G1. After 6 h, cells were harvested and sequentially washed with 50 ml of ice-cold MilliQ water with 0.2 mM PMSF followed by 150 ml buffer A (50 mM HEPES-KOH, pH 7.6, 5 mM MgOAc, 1 mM ZnOAc, 2 mM ATP, 1 mM DTT, 10% glycerol, 0.02% NP-40) supplemented with 0.1 mM EDTA, 0.1 mM EGTA, 0.75 M potassium glutamate (KGLu) and 0.8 M sorbitol. The washed pellet was resuspended in approximately one-third of the packed cell volume of buffer A containing 0.1 mM EDTA, 0.1 mM EGTA, 0.75 M KGLu, 0.8 M Sorbitol, Complete Protease Inhibitor Cocktail Tablet (1 tablet per 15 mL total volume; Roche) and then frozen dropwise in liquid nitrogen. Frozen cells were lysed in a SamplePrep freezermill (SPEX), and the lysate was clarified by ultracentrifugation in a Type 70 Ti rotor at 45,000 r.p.m. for 90 min at 4 °C. The supernatant was applied to 2 ml of anti-M2-Flag resin (Sigma) pre-equilibrated in buffer A containing 0.1 mM EDTA, 0.1 mM EGTA and 0.75 M KGLu and incubated with rotation for 3 h at 4 °C. The resin was collected on a column and the flow-through was discarded. The resin was washed with 20 ml of buffer A with 0.3 M KGLu. Cdt1-Mcm2-7 was eluted with buffer A containing 0.3 M KGLu and 0.15 mg/mL 3 \times FLAG peptide. Peak fractions containing Cdt1-Mcm2-7 were pooled, and the protein was concentrated to ~1 mg/mL using a Vivaspin 6 centrifugal concentrator (molecular weight cutoff, 100 kDa; Sartorius) and aliquoted into 0.8-mL fractions. With an initial cell volume of 8 L, the yield is typically 2 mg of >95% pure Sort-Cdt1-Mcm2-7, according to SDS-PAGE.

SNAP- or CLIP-tagged Cdt1-Mcm2-7 (Cdt1^{SORT}-Mcm2-7^{4SNAP}, Cdt1-Mcm2-7^{25FRET} or Cdt1-Mcm2-7^{25FRET}) was labeled with SNAP-Surface 549 (NEB; Dy549), SNAP-BHQ-2, SNAP-JF646 (a gift from Luke Lavis, Janelia Research Campus) or CLIP-Surface 647 by incubation with 1 nmol of dye at room temperature for 1 h. To make Mcm2-7^{25FRET}-biotin, we followed the procedure for Mcm2-7^{25FRET} but substituted SNAP-549-biotin for SNAP-Surface 549. For SORT-tagged Cdt1-Mcm2-7 (Cdt1^{SORT}-Mcm2-7^{4SNAP}, Cdt1-Mcm2-7^{25FRET} or Cdt1-Mcm2-7^{25quench}), 1 mg of Cdt1-Mcm2-7 was incubated with an equimolar amount of Srt5^o evolved sortase²⁸, and CaCl₂

was added to a final concentration of 5 mM in buffer A with 0.3 M KGLu. This was mixed with 100 nmol of peptide carrying a Sort-tag and labeled with Dy549-maleimide (Dyomics), dissolved in 200 μ L of buffer A with 0.3 M KGLu (the sequences of the peptides used are described below). The reaction was incubated at room temperature for 15 min and then quenched with 20 mM EDTA. The net result of the sortase reaction is coupling of the fluorescently labeled (or biotinylated) peptide to the N terminus of Cdt1 with the sequence NH₂-CHHHHHHHHHHLPETGGG followed by the remainder of the protein or to the C terminus of Mcm2 with the sequence LPETGGGHHHHHHH HHHHC-COOH.

For SNAP or CLIP-tagged Cdt1-Mcm2-7, after the proteins were coupled to fluorophore(s), we applied the reaction to a Superdex 200 10/300 gel filtration column equilibrated in buffer A with 0.1 mM EDTA, 0.1 mM EGTA and 0.3 M KGLu. Peak fractions containing Cdt1-Mcm2-7 were pooled, aliquoted and stored at -80 °C.

For SORT-tagged Cdt1-Mcm2-7, after dye coupling, the reaction was applied to a Superdex 200 10/300 gel filtration column equilibrated in buffer A with 0.1 mM EDTA, 0.1 mM EGTA, 0.3 M KGLu and 10 mM imidazole. Peak fractions containing peptide-coupled Cdt1-Mcm2-7 were pooled and incubated with 0.5 mL of cComplete His-Tag Purification Resin (Roche) pre-equilibrated in buffer A with 0.1 mM EDTA, 0.1 mM EGTA, 0.3 M KGLu, 10 mM imidazole for 1 h with rotation at 4 °C. The flow-through was discarded, and the resin was washed with 5 ml of buffer A with 0.1 mM EDTA, 0.1 mM EGTA, 0.3 M KGLu and 10 mM imidazole. Peptide-coupled Cdt1-Mcm2-7 was eluted using buffer A with 0.1 mM EDTA, 0.1 mM EGTA, 0.3 M KGLu and 0.3 M imidazole. Peak fractions were pooled, aliquoted, and stored at -80 °C.

Special note on handling of fluorescent dyes: light sources on all chromatography apparatuses (AKTA FPLC, HPLC) were turned off during preparative runs. Fractions containing fluorescently labeled peptides and proteins were determined during previous analytical runs.

Fluorescent labeling of peptides for Sortase coupling, as well as purification of the Sortase A pentamutant enzyme and Ulp1, was performed as reported previously⁸.

Percent labeling of Mcm2-7^{25FRET}. To determine the labeling efficiency of the SNAP- and CLIP-tag labeling approaches in the MCM2-7^{25FRET} context, we purified and labeled Mcm2-7^{25FRET} with SNAP-Surface 549 and CLIP-Surface 647 on the Mcm5 and Mcm2 subunits, respectively. We imaged a standard reaction containing 0.25 nM ORC, 1 nM Cdc6 and 2.5 nM Cdt1-Mcm2-7^{25FRET} using the described protocol and monitored the colocalization of Mcm2-7^{25FRET} fluorescence by DNA fluorescence (to ensure that we were monitoring fully assembled complexes). Each colocalization was scored as exhibiting both D and A fluorescence, only D, or only A. By assuming that the labeling reactions of the SNAP and CLIP tags in Mcm2-7^{25FRET} were independent, we calculated from the observed D and A colocalization frequencies that SNAP labeling efficiency was ~74%, and CLIP labeling efficiency was ~81%, yielding ~60% of Mcm2-7^{25FRET} complexes with both D and A fluorophores.

Synthesis of SNAP-549-Biotin and SNAP-BHQ2. Commercially available compounds were used without further purification. Reaction yields were not optimized. Reversed-phase high-performance liquid chromatography (HPLC) was done on an Agilent LC-MS Single Quad System 1200 Series (analytical) and an Agilent 1100 Preparative-scale Purification System (semi-preparative). Analytical HPLC was done on a Waters Atlantis T3 C18 column (2.1 \times 150 mm, 5- μ m particle size) at a flow rate of 0.5 mL/min with a binary gradient from phase A (0.1 M triethyl ammonium bicarbonate (TEAB) or 0.1% trifluoroacetic acid (TFA) in water) to phase B (acetonitrile) and monitored by absorbance at 280 nm. Semi-preparative HPLC was done on a VYDAC 218TP series C18 polymeric reversed-phase column (22 \times 250 mm, 10- μ m particle size) at a flow rate of 20 mL/min. Mass spectra were recorded by electrospray ionization (ESI) on an Agilent 6120 Quadrupole LC-MS, an Agilent 6210 Time-of-Flight (TOF) or a Thermo Scientific QExactive system.

We prepared SNAP-BHQ2 (BG-BHQ2; **Supplementary Fig. 6a**) by reacting the building block BG-NH₂ (New England BioLabs) with commercially available BHQ-2 succinimidyl ester (LGC Biosearch) as described²³. BHQ-2 succinimidyl ester (2.5 mg, 4.1 μ mol) was dissolved in anhydrous DMF (1.0 mL). BG-NH₂ (1.1 mg, 4.1 μ mol) and triethylamine (0.56 μ L, 4.1 μ mol) were added, and the reaction

mixture was incubated at room temperature with stirring overnight. The solvent was removed under vacuum, and the product was purified by reversed-phase HPLC using a 0.1 M TEAB-acetonitrile gradient (yield, 21%). BG-BHQ2: ESI-MS m/z 759.3104 [M+H]⁺ (calculated for C₃₈H₃₈N₁₂O₆, m/z 759.3110).

The bifunctional SNAP-549-biotin (BG-549-biotin; **Supplementary Fig. 6b**) substrate was prepared by successive couplings of commercially available α -N-Fmoc- ϵ -N-Dde-lysine (Merck KGaA) with BG-NH₂ (NEB), N-(+)-biotin-6-aminocaproic acid N-succinimidyl ester (Sigma-Aldrich) and DY-549 acid (Dyomics) according to the synthetic route described by Kindermann *et al.*²⁹ and Smith *et al.*³⁰. SNAP-549-biotin was synthesized as follows: BG-NH₂ (250.0 mg, 0.92 mmol) was dissolved in anhydrous DMF (8 mL). HBTU (N,N,N',N'-tetramethyl-O-(1H-benzotriazol-1-yl)uronium hexafluorophosphate) (368.0 mg, 0.97 mmol), triethylamine (135 μ L, 0.97 mmol), and Fmoc-Lys(Dde)-OH (515.5 mg, 0.97 mmol) were added, and the reaction mixture was maintained at room temperature with stirring overnight. The reaction mixture was poured onto water (80 mL). The white solid was collected by filtration, washed twice with water, and dried in a desiccator under vacuum overnight (yield, 91%). BG-Lys(Dde)-Fmoc (8.0 mg, 10.2 μ mol) was dissolved in anhydrous DMF (1 mL). Et₃NH (3.2 μ L, 30.9 μ mol) was added and the reaction mixture was maintained at room temperature with stirring overnight. The solvent was removed under vacuum. Crude BG-Lys(Dde)-NH₂ was dissolved in anhydrous DMF (1 mL). N-(+)-biotin-6-aminocaproic acid NHS (2.9 mg, 6.4 μ mol) and triethylamine (1.0 μ L, 7.0 mmol) were added, and the reaction mixture was incubated at room temperature with stirring for 1 h. Reaction completion was monitored by LC-MS. A 2% solution of hydrazine in DMF (0.5 mL) was added, and the reaction mixture was incubated at room temperature with stirring for 1 h. The solvent was removed under vacuum, and the product was purified by reversed-phase HPLC with a 0.1% TFA in water-acetonitrile gradient (yield, 76%). BG-Lys(NH₂)-biotin: ESI-TOF-MS m/z 738.3 [M+H]⁺ (calculated for C₃₅H₅₁N₁₁O₅S, m/z 738.4). BG-Lys(NH₂)-biotin-TFA salt (2.3 mg, 2.7 μ mol) was dissolved in anhydrous DMF (1 mL). DY-549 acid (2.7 mg, 3.0 μ mol), HBTU (1.2 mg, 3.0 μ mol) and triethylamine (0.6 μ L, 4.5 μ mol) were added, and the reaction mixture was incubated at room temperature with stirring for 1 h. The solvent was removed under vacuum, and the product was purified by reversed-phase HPLC using 0.1 M TEAB/acetonitrile gradient (yield = 78%). BG-549-PEG-Biotin: ESI-TOFMS m/z 767.7552 [M-2H]²⁻ (calc. for C₆₈H₉₁N₁₃O₁₈S₅, m/z 767.7532).

Single-molecule microscopy. The micro-mirror total internal reflection (TIR) microscope used for multiwavelength single-molecule microscopy with excitation wavelengths of 488, 532 and 633 nm has been described previously^{31,32}. Biotinylated Alexa Fluor 488-labeled 1.3-kb-long DNA molecules containing an origin were coupled to the surface of a reaction chamber with streptavidin. Briefly, the chamber surface was cleaned and derivatized using a 200:1 ratio of mPEG-silane-2000 and biotin-mPEG-silane-3400 (ref. 8). We identified DNA-molecule locations by acquiring four to seven images with 488-nm excitation at the beginning of the experiment. Unless otherwise noted, helicase-loading reactions contained 0.5 nM ORC, 2 nM Cdc6 and 5 nM Cdt1-Mcm2-7. The reaction buffer used was essentially as previously described¹³, but without any glycerol and with the addition of 2 mM dithiothreitol, 2 mg/ml bovine serum albumin (EMD Chemicals; La Jolla, CA), and an oxygen-scavenging system (glucose oxidase and catalase) to minimize photobleaching³². After the addition of protein to the DNA-coupled chamber, frames of 1-s duration were acquired. DNA was imaged before and immediately after adding the reaction to the slide, but not throughout the experiment. The imaging protocol alternated between 1-s frames with the 532-nm laser on and 1-s frames with the 633-nm laser on over 20–30 min. Apparent E_{FRET} values were calculated as described³³.

Because the events observed on each DNA molecule represents an independent measurement of the events being studied, many biological replicates were evaluated in all of the analyses.

Tethering of Mcm2-7 complexes. Tethering experiments were done using Mcm2-7^{25FRET}-biotin in the absence of Cdt1 or Cdt1-biotin with Mcm2-7^{25FRET} purified in the absence of Cdt1. Complexes were added to the slide at a concentration of 0.04 nM, and coupling was briefly visualized. Free complexes were washed out using buffer A with 300 mM Kglut and were imaged for 2 min, alternating between 1-s frames with the 532-nm laser on and 1-s frames with the 633-nm laser on.

Only complexes containing both Alexa Fluor 549 and Alexa Fluor 647 dyes were used for background subtraction and E_{FRET} calculations.

Single-molecule data analysis. Analysis of the CoSMoS data sets was similar to that described in ref. 34. Specifically, we typically followed these four steps³⁵: (1) define the spatial relationship between the two images created at different excitation and emission wavelengths from the single field of view by the dual-view optical system ('mapping'), (2) correct the data set for stage drift that occurred during the experiment ('drift correction'), (3) image the label on origin DNA to identify the locations of single DNA molecules on the surface, and (4) integrate fluorescence emission from small regions centered at the pre-defined locations of coupled DNA locations in each acquired image to obtain plots of fluorescence intensity versus time. We used custom image-processing software (https://github.com/gelles-brandeis/CoSMoS_Analysis) implemented in MATLAB (The Mathworks, Natick, MA) to carry out these steps. Confidence intervals for kinetic data were determined by bootstrapping.

Both dual-imaging optics and chromatic aberrations result in spatial displacement between fluorescent spot images of colocalized species that are labeled with dyes of different colors. Accurate colocalization of the differentially labeled species therefore requires the use of a mapping procedure. For each pair of colors, we acquired a list of several hundred reference spot pairs, using a sample containing a surface-tethered oligonucleotide that was labeled with Alexa Fluor 488, Cy3 and Cy5. We mapped the coordinates of a fluorescent spot to the equivalent location at a different color by using a transformation with fit parameters based on just the 15 nearest reference spots³⁵. Drift correction and spot detection were done as described in ref. 35. Fluorescence emission from labeled complexes was integrated over a 0.37- μ m² area centered at each drift-corrected origin-DNA location, yielding for each DNA molecule a separate intensity time course for each color of fluorescent label being observed.

FRET and quenching data analysis. Images containing spots that were analyzed to produce a FRET time course were first mapped and drift-corrected (see above). By alternating between their laser excitation wavelengths, we monitored the colocalization of donor-labeled and acceptor-labeled Mcm2-7 hexamers with the origin-DNA molecule. To determine the time until formation of the state with $E_{\text{FRET}} \sim 0.36$, we noted the earliest time point at which the E_{FRET} values increased by 0.15 for the first Mcm2-7 or 0.1 for the second Mcm2-7. Only Mcm2-7 molecules that were labeled with both fluorophores were used for analysis of the first Mcm2-7. For analysis of the second Mcm2-7, both the first and the second Mcm2-7 molecules had to be labeled with both fluorophores.

To calculate apparent FRET efficiencies, we first subjected the baseline for each fluorescence intensity trace to a low-pass filter. That smoothed baseline was then subtracted from the starting trace, resulting in a fluorescence time record with a zero mean baseline³¹ (**Fig. 1b**). The apparent FRET efficiency was calculated as follows:

$$E_{\text{FRET}} = \frac{I_{\text{Acceptor}}}{I_{\text{Acceptor}} + I_{\text{Donor}}}$$

where I_{Acceptor} and I_{Donor} are the acceptor and donor emission intensities observed during donor excitation, respectively. No gamma correction was applied because no systematic change in ($I_{\text{Acceptor}} + I_{\text{Donor}}$) was observed upon changes in E_{FRET} (**Fig. 1b** and **Supplementary Fig. 2a**) or upon acceptor photobleaching.

E_{quench} was calculated from baseline-corrected data (of single Mcm2-7 molecules) as described in **Supplementary Figure 4d**.

Measuring FRET values for soluble Mcm2-7^{25FRET}. To generate sufficient loaded Mcm2-7^{25FRET}, we carried out a large-scale helicase-loading reaction with 20 pmol of bead-attached origin DNA, 80 pmol of Mcm2-7^{25FRET}, 20 pmol of ORC, and 40 pmol of Cdc6 (ref. 13). After a 20-min incubation, the DNA beads were washed with a high-salt buffer (to remove incompletely loaded protein), and loaded Mcm2-7^{25FRET} was released from beads by DNase I treatment as previously described¹³. The released, loaded Mcm2-7^{25FRET} or a similar concentration of unloaded solution Cdt1-Mcm2-7^{25FRET} was placed in a cuvette and excited at 549 nm. Fluorescence emission was detected from 560–690 nm, and the peak values

of donor (574 nm) and acceptor (670 nm) emissions were used to determine E_{FRET} values. Reported uncertainties are the s.d. of four separate experiments.

Statistical analysis. Confidence intervals were determined by bootstrapping with either 1,000 samples (Figs. 2 and 4 and Supplementary Figs. 4 and 5) or 250 samples (Supplementary Tables 1–3).

Code availability. Links to code are included in this section, in the legend of Supplementary Figure 3 legend and in the caption of Supplementary Table 1.

Data availability. The data that support the findings of this study are available from the corresponding authors upon reasonable request.

28. Chen, I., Dorr, B.M. & Liu, D.R. A general strategy for the evolution of bond-forming enzymes using yeast display. *Proc. Natl. Acad. Sci. USA* **108**, 11399–11404 (2011).

29. Kindermann, M., Sielaff, I. & Johnsson, K. Synthesis and characterization of bifunctional probes for the specific labeling of fusion proteins. *Bioorg. Med. Chem. Lett.* **14**, 2725–2728 (2004).

30. Smith, B.A. *et al.* Three-color single molecule imaging shows WASP detachment from Arp2/3 complex triggers actin filament branch formation. *eLife* **2**, e01008 (2013).

31. Friedman, L.J. & Gelles, J. Mechanism of transcription initiation at an activator-dependent promoter defined by single-molecule observation. *Cell* **148**, 679–689 (2012).

32. Friedman, L.J., Chung, J. & Gelles, J. Viewing dynamic assembly of molecular complexes by multi-wavelength single-molecule fluorescence. *Biophys. J.* **91**, 1023–1031 (2006).

33. Crawford, D.J., Hoskins, A.A., Friedman, L.J., Gelles, J. & Moore, M.J. Single-molecule colocalization FRET evidence that spliceosome activation precedes stable approach of 5' splice site and branch site. *Proc. Natl. Acad. Sci. USA* **110**, 6783–6788 (2013).

34. Hoskins, A.A. *et al.* Ordered and dynamic assembly of single spliceosomes. *Science* **331**, 1289–1295 (2011).

35. Friedman, L.J. & Gelles, J. Multi-wavelength single-molecule fluorescence analysis of transcription mechanisms. *Methods* **86**, 27–36 (2015).